

# Asymmetric Routings With Fewer Tendons Can Offer Both Flexible Endpoint Stiffness Control and High Force-Production Capabilities in Robotic Fingers

Joshua Inouye and Francisco J. Valero-Cuevas

**Abstract**—The force-production and passive stiffness capabilities of fingers are two critical design specifications for dexterous robotic hands. We used the link and joint kinematic parameters of the 4-DOF DLR index finger to explore the tradeoff between these two design specifications as a function of the number, routing, stiffness, and strength of each tendon. Our innovative computational approach allowed building the Pareto front of optimized passive endpoint stiffness (measured by the eccentricity of the endpoint stiffness ellipsoids) vs. maximal force-production capabilities (measured by the size and shape of the force polytope) for 1,200 randomly generated valid routings with 5, 6, 7, or 8 tendons. Our results show that this parametric optimization can increase realizable isotropic forces by up to 80% compared to the default tendon tension distribution. In addition, designs with 5 or 6 tendons can have endpoint stiffness ellipsoids with optimized low eccentricities and with force production capabilities comparable to designs with 7 or 8 tendons. Interestingly, we did not find a systematic tradeoff between force-production and passive stiffness capabilities, given a specific routing. However, the choice of number, routing and strength of each tendon greatly affects force and passive stiffness capabilities of robotic finger, which reveals the many design opportunities afforded by tendon-driven manipulators and offers insight into the anatomical features of the human musculoskeletal system.

## I. INTRODUCTION

Robotic fingers and hands have been designed for the past few decades for the purposes of grasping and manipulation [1]–[5]. There are many factors involved in the design decisions for these hands, but two important ones are force-production capabilities and passive stiffness. The fingers clearly must be able to generate sufficiently high forces to perform a specific or general task. In addition, the integration of passive stiffness control into the design of robotic hands is important for preventing damage to itself and its surroundings, enabling the ability to perform highly dynamic tasks, and increasing the safety of interacting humans [6]–[8].

Several studies have addressed the problem of identifying the force-production (or more formally, wrench-production) capabilities of both parallel and serial manipulators [9]–[16]. According to [11], “The knowledge of maximum twist and

wrench capabilities is an important tool for achieving the optimum design of manipulators”. Two common approaches to the problem of quantifying these capabilities are manipulating force ellipsoids (which apply accurately only to torque-driven systems) and force polytopes (also known as feasible force sets, which apply exactly to tendon driven systems [17]. From these force-production capabilities, a performance metric can then be assigned based on the size and/or shape of the ellipsoid or polytope.

For tendon-driven robotic fingers, one key design element is the tendon routing, which defines the structure matrix, of the finger. This structure matrix defines the torque and force produced by the finger based on tensions of the tendons. Certain studies have addressed the problem of designing a structure matrix for isotropic force transmission characteristics (i.e., ability to transmit forces equally in all directions at the end effector) [18]–[23]. However, these studies have not considered the distribution of maximal tensions across tendons, which is certainly important in small, dexterous hands where weight and size minimization are significant priorities. Altering the maximal tendon tension distribution in tendon-driven hands is known to have a significant effect on force-production capabilities [24], [25]. Additionally, the number of tendons used in the design is fundamental to the design of the structure matrix, and using fewer tendons “has the advantage of reducing the number of tendons and actuators and therefore reduces the weight, size, and complexity of the manipulator...” [18].

The importance of stiffness control of manipulators has been widely recognized in the literature [4], [6]–[8], [26]–[29]. Manipulators can have active or passive stiffness control, or a combination of both. Active stiffness control can be programmed using a feedback control law [27], but is limited by the control loop frequency, and a sudden impact to the manipulator can cause damage to the robot or its surroundings before the control loop is activated to absorb the energy [4]. Thus, passive stiffness is also important, especially in unstructured environments where unexpected obstacles, objects, or humans may make contact with the manipulator. Passive stiffness control is typically implemented by variable-stiffness actuators [6], [7], [30]–[34]. Synthesis of endpoint stiffness for serial manipulators with adjustable joint stiffnesses is studied in [35]. An extensive analysis of the joint stiffness matrices for tendon-driven manipulators is conducted in [34].

Therefore, it is clearly desirable to design a robotic

This material is based upon work supported by NSF Grant 0836042, NIDRR Grant 84-133E2008-8, and NIH Grant AR050520 and Grant AR052345 to FVC.

J. Inouye is with the Department of Biomedical Engineering, University of Southern California, CA, 90089 USA. e-mail: jinouye@usc.edu.

F. J. Valero-Cuevas is with the Department of Biomedical Engineering & the Division of Biokinesiology and Physical Therapy, University of Southern California. e-mail: valero@usc.edu

hand with both adequate passive stiffness and high force-production capabilities. In addition, it can be beneficial to design a finger with as few tendons as possible. Utilizing computational methods and applying theoretical analyses, we quantify the ability of 1,200 tendon routings to produce maximal isotropic forces and endpoint stiffness ellipsoids with low eccentricity. This novel approach enables the systematic exploration of the design space. For example, we show that fewer tendons does not imply worse passive stiffness, but designs with fewer tendons typically cannot produce as much isotropic force as designs with more tendons. Tuning tendon stiffnesses can lead to endpoint stiffness ellipsoids with low eccentricity, and adjusting the distribution of maximal tension across tendons can lead to large increases in isotropic force-production capabilities. Our study demonstrates, to the best of our knowledge, the first practical computational exploration of the effect of tendon routing simultaneously on these two characteristics.

## II. METHODS

The minimal number of tendons required to fully control all of the degrees of freedom (DOFs) of an  $n$ -joint robotic finger is  $n + 1$  [23]. Because tendons have unidirectional actions (i.e., they can only pull), this minimal number of tendons must also be routed judiciously [17]. A finger with this many tendons employs what is called an “N+1” design. The DLR finger and most anthropomorphic fingers have 4 DOFs (that do not use coupled joints), which means that the minimal number of tendons for full controllability of the finger is 5. However, many hands have been designed using a “2N” design, which uses a number of tendons equal to 2 times the DOFs—with a pair of agonist-antagonist tendons dedicated to each joint [1], [3], [4]. In general, increasing the number of tendons beyond 2N is impractical or undesirable for robotic fingers because of size constraints<sup>1</sup>. In addition, any number of tendons between N+1 and 2N may be used. We carried out analyses on 4 categories of designs: having 5 (N+1), 6 (N+2), 7 (N+3), or 8 (2N) tendons.

The routing and moment arms of tendons in a finger are critical, and can be mathematically described by an  $n \times m$  structure matrix (also called a moment arm matrix)  $R$ , where  $n$  is the number of DOFs of the finger and  $m$  is the number of tendons. The entries  $r_{i,j}$  are signed moment arm values for the  $i^{\text{th}}$  joint and  $j^{\text{th}}$  tendon [37]. For simulation purposes, we randomly selected 300 admissible structure matrices from each of the tendon categories by randomizing the signs of the non-zero entries and then checking for controllability conditions<sup>2</sup> as described in [20]. This process is shown in Fig. 1, with the non-zero entries represented by ‘#’. The number of admissible structure matrices for all categories combined is 222,208 (using a combinatoric search of the ‘#’ entries in Fig. 1 for each category). Therefore, evaluating all

<sup>1</sup>However, most vertebrate limbs have more than 2N muscles—which is a subject of continual debate. See [17], [36]

<sup>2</sup>The basic idea behind the controllability conditions is that each joint can be actuated independently in torque and motion, given that tendons can only pull and not push.

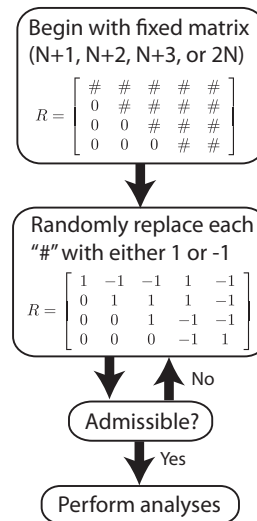


Fig. 1. Procedure for finding admissible structure matrices. N+1 structure matrix shown.

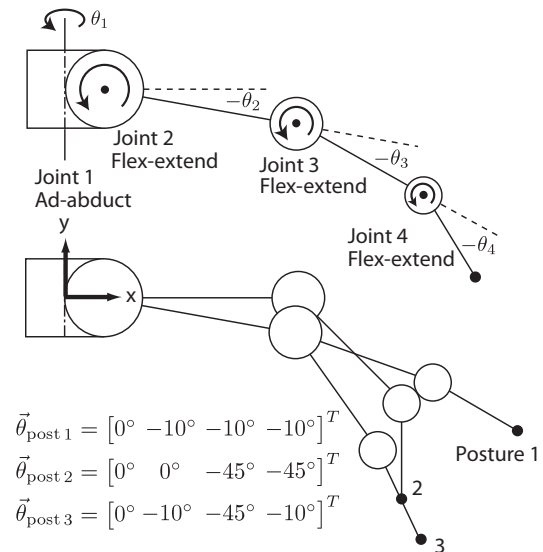


Fig. 2. Postures analyzed for each tendon routing. Link lengths and joint diameters shown to scale (i.e., with kinematic parameters of the DLR hand).

of these designs is relatively intractable for our purposes and we deemed that randomly selecting 300 from each category for a total of 1,200 evaluated routings was sufficient to prove the point of this study.

To compare and contrast the force-production and stiffness capabilities of various finger designs, we identified a fitness metric describing each aspect. We calculated these metrics at 3 different postures for each of the 1,200 routings, and averaged the metrics over the 3 postures, which are shown in Fig. 2.

The fitness metric used for stiffness control was the ESE (endpoint stiffness eccentricity) and the metric used for force production was the MIV (maximal isotropic value). The calculation of these metrics is described in the next sections.

### A. Analysis and Synthesis of Stiffness

1) *Joint Stiffness Adjustability*: The endpoint Cartesian stiffness matrix,  $K_{end}$ , relates the endpoint displacements (from an equilibrium position),  $\vec{\partial}x$ , to endpoint forces,  $\vec{F}$ , as shown in the following equation:

$$\vec{F}_{end} = -K_{end}\vec{\partial}x \quad (1)$$

The joint stiffness matrix,  $K_{joint}$ , relates the joint displacements (from an equilibrium position),  $\vec{\partial}\theta$ , to joint torques,  $\vec{\tau}$ , as shown in the following equation:

$$\vec{\tau} = -K_{joint}\vec{\partial}\theta \quad (2)$$

The endpoint stiffness matrix can be found from the joint stiffness matrix using the following well-known equation [38]–[42]:

$$K_{end} = J^{+T} \left( K_{joint} - \frac{\partial J^T}{\partial \vec{\theta}} \vec{F}_{tip} \right) J^+ \quad (3)$$

where  $J$  is the posture-dependent Jacobian relating joint angle velocities to endpoint velocities,  $J^+$  is the Moore-Penrose pseudoinverse of  $J$  (if the manipulator is redundant, as is the case in this study), and  $\vec{F}_{tip}$  is the external force vector on the tip of the finger. The joint stiffness matrix for a tendon-driven finger may be found from the structure matrix  $R$  and the diagonal tendon stiffness matrix  $K_t$  using the following equation [43]:

$$K_{joint} = RK_tR^T \quad (4)$$

For the purposes of this computational study, we assume that the external force on the fingertip is zero. However, similar computational studies could be conducted with an external fingertip force. Combining Eqs. 3 and 4 with the external force being zero, we get the endpoint stiffness matrix as a function of tendon stiffnesses and tendon routing:

$$K_{end} = J^{+T} (RK_tR^T) J^+ \quad (5)$$

For the DLR index finger in an unloaded configuration (Eq. 3 changes if there is a constant load applied to the endpoint [43]),  $K_{end}$  is a  $3 \times 3$  symmetric, positive semi-definite matrix,  $K_{joint}$  is a  $4 \times 4$  symmetric, positive semi-definite matrix,  $J$  is a  $3 \times 4$  matrix,  $R$  is a  $4 \times m$  matrix ( $m$  is the number of tendons ranging from 5-8), and  $K_t$  is an  $m \times m$  diagonal matrix.

We can see clearly from Eq. 3 that the endpoint stiffness is a function of joint stiffness, and that realizing a completely arbitrary endpoint stiffness can be difficult in general due to the multiplication by the Jacobian and the inversions involved. Depending on the configuration, it may or may not be possible to realize an arbitrary endpoint stiffness matrix [35] because of the constraint that the joint stiffness matrix must be positive definite. It can be noted that an arbitrary 3-D endpoint stiffness matrix involves 6 free parameters. Therefore, if there are not at least 6 free parameters in the

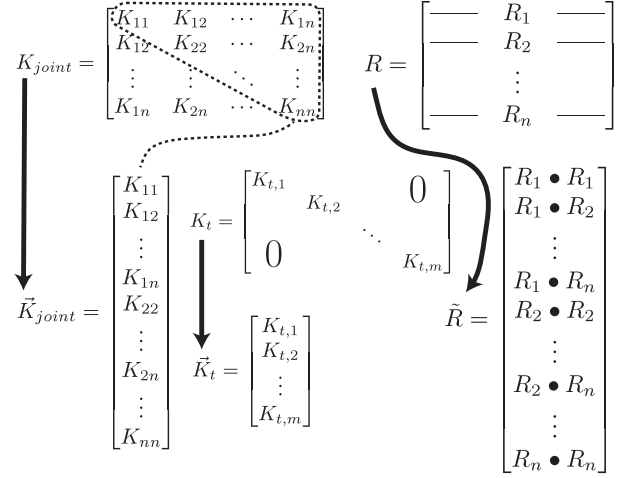


Fig. 3. Reformulation of variables in Eq. 4 for use in Eq. 6. (•) denotes element-by-element multiplication.  $R_i$  is the  $i^{th}$  row of  $R$ . Joint stiffness adjustability (JSA) is equal to  $\text{rank}(\tilde{R})$ .

joint stiffness matrix, it is not possible to realize an arbitrary endpoint stiffness.

For the 4-DOF DLR finger, the joint stiffness matrix is  $4 \times 4$ , and so there are 10 free parameters. Reformulating Eq. 4 enables quantification of the *joint stiffness adjustability* (JSA), which can be interpreted as the flexibility of realizing a joint stiffness matrix for a specific routing when tendon stiffness selection is arbitrary. The reformulation [34] involves rearranging the independent parameters of the joint stiffness matrix into a vector, which is then a linear function of the tendon stiffness, also rearranged into a vector:

$$\vec{K}_{joint} = \tilde{R}\vec{K}_t \quad (6)$$

where  $\vec{K}_{joint}$ ,  $\tilde{R}$ , and  $\vec{K}_t$  are reformulated as shown in Fig. 3. (•) denotes element-by-element multiplication, and  $R_i$  is the  $i^{th}$  row of  $R$ . Note that  $\vec{K}_{joint}$  has length  $n(n+1)/2$  (where  $n$  is the number of DOFs of the finger),  $\tilde{R}$  is an  $n(n+1)/2 \times m$  matrix (where  $m$  is the number of tendons of the finger), and  $\vec{K}_t$  has length  $m$ , and all of its elements must be positive. Mathematically, the rank of  $\tilde{R}$  is the number of free parameters of the joint stiffness matrix that can be independently chosen. Of course, the tendon stiffnesses must be positive, and the range of realizable joint stiffnesses is constrained by a particular routing, but this is nevertheless an estimation of the freedom in choosing an arbitrary joint stiffness matrix [34], which in turn affects the freedom to choose an arbitrary endpoint stiffness matrix. The rank of  $\tilde{R}$  is the joint stiffness adjustability (JSA):

$$\text{JSA} = \text{rank}(\tilde{R}) \quad (7)$$

Note again that this measure assumes that each tendon stiffness can be independently chosen, regardless of tendon tension.

2) *Endpoint Stiffness Eccentricity*: As suggested above, higher JSA will, in general, translate to a larger set of realizable endpoint stiffnesses. We quantify the ability of a specific routing to realize an endpoint stiffness ellipsoid<sup>3</sup> with low eccentricity by formulating the following optimization problem:

$$\begin{aligned} & \underset{K_t}{\text{minimize}} && \kappa(K_{end}) \\ & \text{subject to} && K_t \geq 0 \end{aligned}$$

where  $\kappa(\cdot)$  denotes the condition number: the ratio of the largest to the smallest singular values of the matrix. It is a measure of the eccentricity of the endpoint stiffness ellipsoid [44]. We will call this the *endpoint stiffness eccentricity*, or ESE.

$$\text{ESE} = \kappa(K_{end}) \quad (8)$$

We implemented the above optimization in Matlab using the ‘fmincon’ command. Condition number minimization is a difficult problem in general [45]–[47]. It is quasi-convex over the entries of the matrix, but the entries of the matrix are non-convex functions of the elements of  $\vec{K}_t$  in our problem due to the matrix inversions. However, taking the best result from 5 random starting points in the positive unit hypercube (i.e., positive orthant) seemed to give good, repeatable results. The optimized endpoint stiffness eccentricity, ESE\*, quantifies the eccentricity of the best-conditioned stiffness ellipsoid that the optimization was able to find. It can be noted that minimizing the eccentricity of the ellipsoid is equivalent to maximizing its isotropy. A perfectly spherical stiffness ellipsoid has a condition number of 1.

### B. Analysis and Optimization of Force Polytopes

The feasible force set is the convex polytope of all forces that can be exerted by the endpoint of a tendon-driven finger, given a posture, tendon routing, and maximal tendon tensions [10], [16], [24]. Any force vector outside of this 3-D set (or 2-D set, for planar analyses) cannot be achieved by the endpoint. A quality metric that can be assigned to this set is known as the maximal isotropic value (MIV) [12]. It is the radius of the largest ball, centered at the origin, that the feasible force set can contain. A finger can exert at least that many units of force in any direction.

To find the feasible force set, we first specify the posture (which allows computation of the Jacobian  $J$ ) and tendon routing  $R$  of the finger. These matrices involve the following relations:

$$\dot{x} = J\dot{\theta} \quad (9)$$

$$\vec{\tau} = R\vec{T} \quad (10)$$

<sup>3</sup>The stiffness ellipsoid is formed by projecting a unit sphere from differential displacements to differential endpoint forces using the linear transformation  $K_{end}$ , as in Eq. 1. It assumes infinitesimal displacements that have negligible effects on the Jacobian matrix. Large displacements will not be as accurately represented by ellipsoids due to larger changes in the Jacobian matrix.

where  $\dot{x}$  is the endpoint translational velocity vector,  $\dot{\theta}$  is the joint velocity vector, and  $\vec{T}$  is the vector of tendon tensions.

We can use an activation vector,  $\vec{a}$ , to represent the degree to which a tendon is activated. Each element of  $\vec{a}$  ranges between 0 (no activation) and 1 (full activation). Further discussion may be found in [48]. If we define  $T_{max}$  as a diagonal matrix of maximal tendon tensions, then we get the following relation between activations and tendon tensions:

$$\vec{T} = T_{max}\vec{a} \quad (11)$$

If we combine Eqs. 10 and 11, then we get:

$$\vec{\tau} = RT_{max}\vec{a} \quad (12)$$

The feasible 3-D force set can be found from this feasible torque set by intersecting the feasible torque set with the linear subspace spanned by the columns of  $J^T$  [49]. The vertices of this reduced-dimensionality set can then be transformed to vertices in endpoint force space:

$$\vec{F} = J^{+T}\vec{\tau} \quad (13)$$

where  $J^{+T}$  denotes the Moore-Penrose pseudoinverse of  $J^T$ . The convex hull of all of these vertices in force space is a polytope and defines the feasible force set. We use the Quickhull algorithm [50] implemented in the Qhull software package to find the MIV.

Different routings and maximal tendon tensions both affect the size and shape of the feasible torque set shown in Eq. 12, which in turn affects the size and the shape of the feasible force set. If we have a fixed routing and posture, then we can change the feasible force set and MIV by varying the maximal tendon tensions (given by diagonal matrix  $T_{max}$ ). If we constrain the sum of the maximal tendon tensions to be constant (a reasonable constraint due to the size and weight constraints inherent in dexterous hands [24]), then we can optimize the MIV using the following formulation:

$$\begin{aligned} & \underset{F_0}{\text{maximize}} && \text{MIV} = f(J, R, T_{max}) \\ & \text{subject to} && T_{max} \geq 0, \\ & && \text{trace}(T_{max}) = T_{\text{max sum}} \end{aligned}$$

where  $T_{\text{max sum}}$  is a constant.

Evaluating the MIV given  $J$ ,  $R$ , and  $T_{max}$  is fairly expensive computationally when compared with function evaluations for the stiffness problem. Therefore, we utilized a custom, greedy Markov-Chain Monte Carlo optimization algorithm which was fairly effective at finding a local maximum within 300 iterations. We denote this maximum by MIV\*.

It is worth noting that MIV is a function of  $J$ ,  $R$ , and  $T_{max}$ , while the ESE is a function of  $J$ ,  $R$ , and  $K_t$ . Therefore, changes in  $T_{max}$  will not affect the ESE and changes in  $K_t$  will not affect the MIV. However, the Jacobian matrix and the routing have effects on *both* of these characteristics. This study is focused mostly on the effects of *routing* on these two characteristics. It can also be noted that with a torque-driven

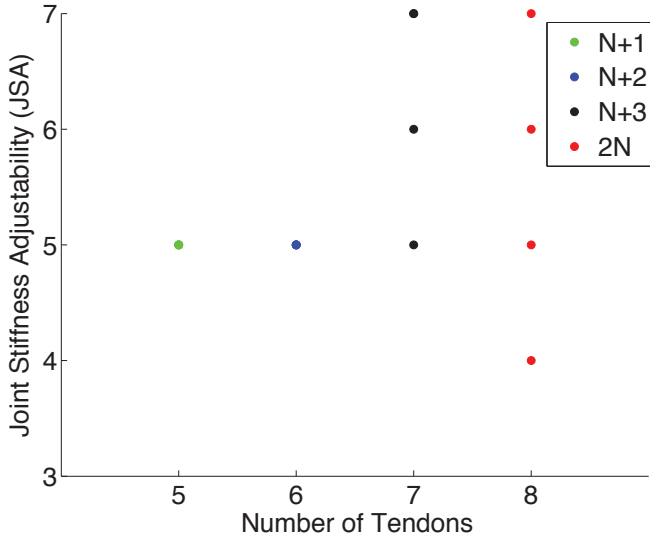


Fig. 4. Joint stiffness adjustability versus number of tendons, plotted for all admissible routings. Mathematically, JSA is the rank of  $\bar{R}$ , which is the number of free parameters of the joint stiffness matrix that can be independently chosen.

manipulator, the analysis of force production and stiffness synthesis becomes much less interesting, as there are very few design parameters that can be altered compared with the tendon-driven manipulator. Furthermore, torque-driven manipulators are not able to utilize the advantages of tendon-driven manipulators as stated in the introduction.

### III. RESULTS

#### A. Joint Stiffness Adjustability

We were able to determine the JSA of all 222,208 admissible tendon routings. The results are shown in Fig. 4. We see that designs with 5 or 6 tendons have a JSA of 5, while designs with 7 or 8 tendons can have a JSA of up to 7 (but never 8!). However, some designs with 8 tendons can only have a JSA of 4, which corresponds to symmetric routings (a  $2N$  design where the moment arms of one tendon are the opposite sign and equal magnitude of those from another tendon), as noted in [34]. A symmetric routing which controls all of the degrees of freedom of an  $N$ -DOF manipulator requires at least  $2N$  tendons, so routings of a 4-DOF finger with 5, 6, or 7 tendons cannot be symmetric.

#### B. Optimized Endpoint Stiffness Eccentricity vs. Maximal Isotropic Value

For the 300 randomly-selected routings from each category, we found the  $ESE^*$  (optimized ESE) and the unoptimized MIV, shown in Fig. 5. The MIV was calculated with all maximal tendon tensions being equal and the sum being constant at 1000N. We did not optimize the MIV for every design due to computational tractability considerations and because it is not crucial for the purposes of this study. (See below for some examples of optimized MIV).

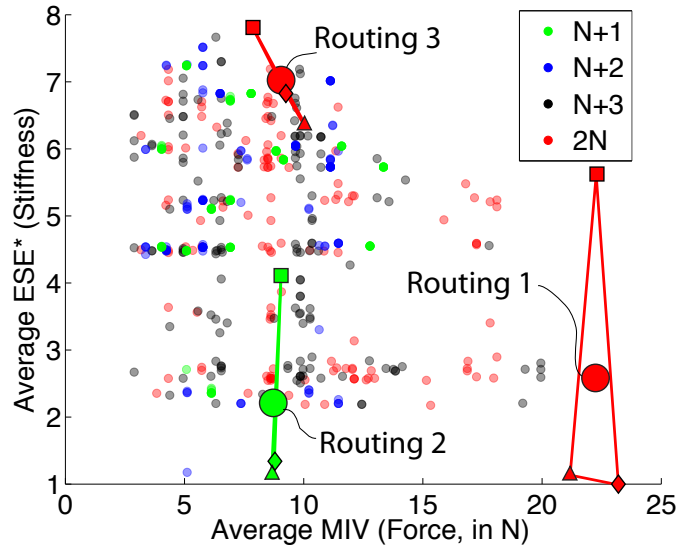


Fig. 5. Optimized endpoint stiffness eccentricity ( $ESE^*$ ) vs. unoptimized maximal isotropic value (MIV), averaged over the 3 postures. Note: only 524 out of 1,200 data points shown (all other designs had higher  $ESE^*$  than 8 and lower MIV than 16). Large circles mark the averages of posture 1 (small squares), posture 2 (small triangles), and posture 3 (small diamonds) for the routings shown in Fig. 6.

We see that, in general, the best routings with 7 or 8 tendons have a substantially higher (unoptimized) MIV than the best routings with 5 or 6 tendons. However, routings with fewer tendons are not less able to produce low  $ESE$  values.

#### C. Optimizing MIV for 3 Specific Routings

To demonstrate that optimization of MIV is possible, we did optimize the MIV, in posture 2, for the three routings marked with large circles in Fig. 5. Routing 1 is the one with the highest unoptimized MIV, and it has 8 tendons. Routing 2 was chosen as an  $N+1$  design that had both low average  $ESE^*$  and high MIV compared with other  $N+1$  designs. Routing 3 was chosen as a reference point, having a mathematically even, symmetric moment arm matrix of a  $2N$  design (the matrix values are only indicative of the sign of the moment arm and not the magnitude):

$$R_{\text{ROUTING 3}} = \begin{bmatrix} 1 & -1 & 1 & -1 & 1 & -1 & 1 & -1 \\ 0 & 0 & 1 & -1 & 1 & -1 & 1 & -1 \\ 0 & 0 & 0 & 0 & 1 & -1 & 1 & -1 \\ 0 & 0 & 0 & 0 & 0 & 0 & 1 & -1 \end{bmatrix}$$

The optimization was able to improve the MIV in posture 2 from 21.2N to 26.0N for Routing 1 (a 23% increase), from 8.68N to 15.6N for Routing 2 (an 80% increase), and from 10.0N to 18.0N for Routing 3 (an 80% increase). Fig. 6 shows the routings, unoptimized feasible force sets, optimized feasible force sets, unoptimized endpoint stiffness ellipsoids (with all tendons having equal stiffnesses), and optimized endpoint stiffness ellipsoids. Two 3-D views are shown of the feasible force sets. The optimized tendon stiffness values shown are normalized so that the highest

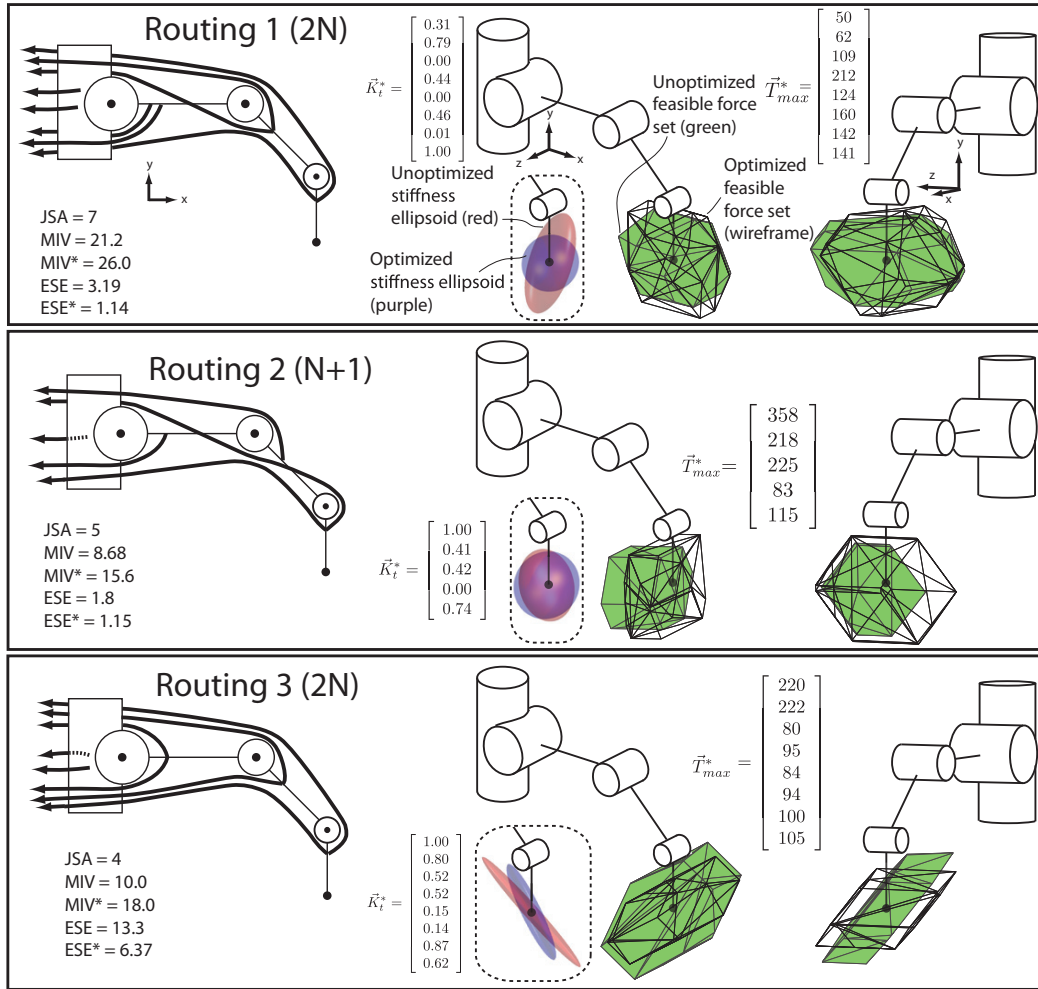


Fig. 6. Illustration of 3 routings along with stiffness ellipsoids and feasible force sets. JSA: Joint stiffness adjustability. MIV: Maximal isotropic value before optimization, in N. MIV\*: Maximal isotropic value after optimization, in N. ESE: Endpoint stiffness eccentricity before optimization. ESE\*: Endpoint stiffness eccentricity after optimization.  $\vec{K}_t^*$ : tendon stiffnesses producing ESE\*, normalized so that maximal stiffness is 1.  $\vec{T}_{max}^*$ : maximal tendon tensions producing MIV\*, in N. Note: all results shown are for posture 2 only, and values correspond with the small triangles in Fig. 5.

stiffness has a value of 1 (multiplying all the stiffnesses by a scalar does not affect the condition number).

We see that routings 1 and 2 are able to produce very low ESE\* values, while Routing 3 is only able to produce an ESE\* of 6.37 (in posture 2). It can be noted that some of the optimized tendon stiffnesses are 0, which may only be realizable in practice with a direct drive DC motor actuator (in which case also the motor inertia would not necessarily allow for instantaneous extension of the tendon with zero resistance). However, we feel that this is not extremely important in our simulation results and general conclusions, since this analysis and optimization could easily be implemented with additional constraints (such as minimal and maximal values for tendon stiffnesses).

We can also observe in Routing 1 that the two tendons that only cross the first joint could be easily combined into one tendon in strength and stiffness, resulting in a routing with 7 tendons that has the exact same characteristics as the routing shown with 8 tendons.

#### IV. DISCUSSION

The main purpose of this study was to demonstrate the large effect of tendon routing, number, and properties on force-production and stiffness realization capabilities. We show that tendon routings with fewer than 2N tendons (which are necessarily asymmetric) can have high force-production capabilities as well as low eccentricity of endpoint stiffnesses.

Our optimization of the endpoint stiffness assumed that it is desirable to produce nearly-isotropic endpoint stiffness, as we assumed no knowledge about the task or potential obstacles to the fingertip. In some practical cases, it may be desirable to adjust the endpoint stiffness characteristics asymmetrically according to the task or situation [6] to be compliant in one direction and stiff in another. For example, if the task is to push a button, guide a rod, etc, then it may be beneficial to have high stiffness in the direction of force application but low stiffness in the directions perpendicular to the direction of force application. Any specific task re-

quirements could easily be incorporated into an optimization routine.

For any practical application, the analyses used in this study would need to take into account the actuation system, and whether it incorporates non-linear or adjustable stiffnesses. The calculation of JSA and the optimization of ESE and MIV in this study assume that the tendon stiffnesses can be controlled independently of tendon tension and that the stiffnesses are linear.

Even if the actuation scheme used in a physical system does not allow for tendon stiffness control apart from tendon tension, the analyses used here could be used to guide the designation of spring constants for linear springs in series with actuators (i.e., some tendons could use stiff springs and others more compliant springs for a desired generic endpoint stiffness). Non-linear springs [30] could be designed also with varying properties among tendons (e.g., with different elasticity constants and biases [34]).

While the MIV was used as the fitness metric for the force-production capabilities, some hands or fingers may only need strong flexing force for use in grasping and the maximal extension force requirements may be low. In this case, the distribution of maximal tendon tensions could be adjusted or optimized according to grasping or other task requirements [24], possibly significantly reducing the total weight or volume of the actuation system when compared with only using identical actuators for all tendons. Also, if non-linear stiffnesses are used in series with actuators, then the calculation of feasible force sets may need to be adjusted to account for the fact that pre-tension (possibly very high) will need to be applied to obtain a desired stiffness.

We only analyzed routings where the tendons routed around every joint that they passed (i.e., that the structure matrix is pseudo-triangular, as in [20]) and where all moment arms were equal in magnitude for a particular joint. We acknowledge that many of the routings that we analyzed may not be realizable in practice. Routings can be designed where tendons pass through the center of joints [33], or where moment arms for different tendons on the same joint can have different magnitudes. Varying moment arms can add more potential flexibility to force-production and stiffness characteristics, while on the other hand, practical design considerations may preclude realization of some routings. However, the analyses could be run on a set of practical routings, spring stiffnesses, and maximal tendon tensions to guide in the design process.

While we have analyzed the passive control of stiffness and the bounds of force production in a finger, we have not considered directly the consequences of finger design to active control, which is of huge importance when constructing a useful system. In addition, a physical system subject to friction, estimation errors, actuator inconsistencies, and other factors may mandate certain design constraints that we have not analyzed.

Lastly, it is natural to compare our results to the number, routing and strength of the musculotendons of the human index finger. That index finger has 4 DOFs, and 7 tendons

(6 tendons for the middle and ring fingers) [16], [51]. Interestingly, that anatomy has fewer than  $2N$  actuators and exhibits cross-over tendons such as those seen in Routings 1 and 2. In addition, muscles have different strengths and stiffnesses (muscles with longer tendons are naturally more compliant). Future work will apply this analysis to the anatomy of biological fingers.

In this study we have shown that there is a very wide range of force-production and stiffness capabilities of different tendon routings with varying numbers of tendons. We feel that the methods presented here could be used to guide in the design process for tendon-driven fingers, hands, or other manipulators, to maximize force production for various tasks, minimize the size and weight of the actuation system, and design tendon stiffness characteristics to realize various joint and endpoint stiffnesses. Furthermore, analysis of the human musculoskeletal system from the perspective of stiffness control and force-production simultaneously could elucidate the advantages and disadvantages of its anatomical features.

## V. ACKNOWLEDGMENTS

The authors gratefully acknowledge the help of M. Grebenstein in providing the kinematic parameters for the DLR index finger and the helpful discussions with J. Kutch, S. Schaal, M. Kurse, and P. Pastor.

## REFERENCES

- [1] S. Jacobsen, E. Iversen, D. Knutti, R. Johnson, and K. Biggers, "Design of the utah/mit dextrous hand," 1986, pp. 1520–1532, 1986 IEEE International Conference on Robotics and Automation. Proceedings.
- [2] J. K. Salisbury and J. J. Craig, "Articulated hands: Force control and kinematic issues," *The International Journal of Robotics Research*, vol. 1, no. 1, p. 4, 1982.
- [3] Shadow Dexterous Hand, Shadow Robot Company.
- [4] M. Grebenstein, A. Albu-Schffer, T. Bahls, M. Chalon, O. Eiberger, W. Friedl, R. Gruber, U. Hagn, R. Haslinger, and H. Hppner, "The dlr hand arm system," *Submitted to ICRA*, vol. 11.
- [5] R. O. Ambrose, H. Aldridge, R. S. Askew, R. R. Burrige, W. Bluethmann, M. Diftler, C. Lovchik, D. Magruder, and F. Rehnmark, "Robonaut: Nasa's space humanoid," *IEEE Intelligent Systems and Their Applications*, vol. 15, no. 4, pp. 57–63, 2000.
- [6] S. Wolf and G. Hirzinger, "A new variable stiffness design: Matching requirements of the next robot generation." IEEE, 2008, pp. 1741–1746, robotics and Automation, 2008. ICRA 2008. IEEE International Conference on.
- [7] G. A. Pratt and M. M. Williamson, "Series elastic actuators." Published by the IEEE Computer Society, 1995, p. 399, iros.
- [8] M. Grebenstein and P. van der Smagt, "Antagonism for a highly anthropomorphic handarm system," *Advanced Robotics*, vol. 22, no. 1, pp. 39–55, 2008.
- [9] S. Bouchard, C. M. Gosselin, and B. Moore, "On the ability of a cable-driven robot to generate a prescribed set of wrenches." Citeseer, proc. of the ASME International Design Engineering Technical Conferences, Mechanics and Robotics Conference.
- [10] P. Chiacchio, Y. Bouffard-Vercelli, and F. Pierrot, "Force polytope and force ellipsoid for redundant manipulators," *Journal of Robotic Systems*, vol. 14, no. 8, pp. 613–620, 1997.
- [11] F. Firmani, A. Zibil, S. B. Nokleby, and R. P. Podhorodeski, "Wrench capabilities of planar parallel manipulators. part i: Wrench polytopes and performance indices," *Robotica*, vol. 26, no. 06, pp. 791–802, 2008.
- [12] R. Finotello, T. Grasso, G. Rossi, and A. Terribile, "Computation of kinetostatic performances of robot manipulators with polytopes," vol. 4. IEEE, 1998, pp. 3241–3246, robotics and Automation, 1998. Proceedings. 1998 IEEE International Conference on.

- [13] M. Gouttefarde and S. Krut, "Characterization of parallel manipulator available wrench set facets," *Advances in Robot Kinematics: Motion in Man and Machine*, pp. 475–482, 2010.
- [14] A. Zibil, F. Firmani, S. B. Nokleby, and R. P. Podhorodeski, "An explicit method for determining the force-moment capabilities of redundantly actuated planar parallel manipulators," *Journal of mechanical design*, vol. 129, p. 1046, 2007.
- [15] L. Kuxhaus, S. S. Roach, and F. J. Valero-Cuevas, "Quantifying deficits in the 3d force capabilities of a digit caused by selective paralysis: application to the thumb with simulated low ulnar nerve palsy," *Journal of Biomechanics*, vol. 38, no. 4, pp. 725–736, 2005.
- [16] F. J. Valero-Cuevas, F. E. Zajac, and C. G. Burgar, "Large index-fingertip forces are produced by subject-independent patterns of muscle excitation," *Journal of Biomechanics*, vol. 31, no. 8, pp. 693–704, 1998.
- [17] F. J. Valero-Cuevas, H. Hoffmann, M. U. Kurse, J. J. Kutch, and E. A. Theodorou, "Computational models for neuromuscular function," *IEEE Reviews in Biomedical Engineering (2) October*, pp. 110–135, 2009.
- [18] L. W. Tsai, "Design of tendon-driven manipulators," *Journal of mechanical design*, vol. 117, p. 80, 1995.
- [19] J. B. Sheu, J. J. Huang, and J. J. Lee, "Kinematic synthesis of tendon-driven robotic manipulators using singular value decomposition," *Robotica*, vol. 28, no. 01, pp. 1–10, 2009.
- [20] J. J. Lee and L. W. Tsai, "The structural synthesis of tendon-driven manipulators having a pseudotriangular structure matrix," *The International Journal of Robotics Research*, vol. 10, no. 3, p. 255, 1991.
- [21] D. Z. Chen, J. C. Su, and K. L. Yao, "A decomposition approach for the kinematic synthesis of tendon-driven manipulators," *Journal of Robotic Systems*, vol. 16, no. 8, pp. 433–443, 1999.
- [22] Y. J. Ou and L. W. Tsai, "Isotropic design of tendon-driven manipulators," *Journal of mechanical design*, vol. 118, no. 3, pp. 360–366, 1996.
- [23] —, "Kinematic synthesis of tendon-driven manipulators with isotropic transmission characteristics," *Journal of mechanical design*, vol. 115, p. 884, 1993.
- [24] N. S. Pollard and R. C. Gilbert, "Tendon arrangement and muscle force requirements for humanlike force capabilities in a robotic finger," *environment*, vol. 17, p. 14, 2002.
- [25] J. M. Inouye, J. J. Kutch, and F. Valero-Cuevas, "Quantitative prediction of grasp impairment following peripheral neuropathies of the hand," *Proceedings of the 35th Annual Meeting of the American Society of Biomechanics, Long Beach, CA, 2011.*, 2011.
- [26] M. Hashimoto and Y. Imamura, "Design and characteristics of a parallel link compliant wrist." IEEE, 1994, pp. 2457–2462 vol. 3, robotics and Automation, 1994. Proceedings., 1994 IEEE International Conference on.
- [27] N. Hogan, "Impedance control—an approach to manipulation. i-theory. ii-implementation. iii-applications," *ASME Transactions Journal of Dynamic Systems and Measurement Control B*, vol. 107, pp. 1–24, 1985.
- [28] C. Ott, *Cartesian impedance control of redundant and flexible-joint robots*. Springer Verlag, 2008, vol. 49.
- [29] G. P. Starr, "Cartesian stiffness control of the jpl/stanford/salisbury hand." IEEE, 1988, pp. 636–637 vol. 1, robotics and Automation, 1988. Proceedings., 1988 IEEE International Conference on.
- [30] K. F. Laurin-Kovitz, J. E. Colgate, and S. D. R. Carnes, "Design of components for programmable passive impedance." IEEE, 1991, pp. 1476–1481 vol. 2, robotics and Automation, 1991. Proceedings., 1991 IEEE International Conference on.
- [31] T. Wimbock, C. Ott, A. Albu-Schaffer, A. Kugi, and G. Hirzinger, "Impedance control for variable stiffness mechanisms with nonlinear joint coupling." IEEE, 2008, pp. 3796–3803, intelligent Robots and Systems, 2008. IROS 2008. IEEE/RSJ International Conference on.
- [32] S. Sugano, S. Tsuto, and I. Kato, "Force control of the robot finger joint equipped with mechanical compliance adjuster," vol. 3. IEEE, 1992, pp. 2005–2013, intelligent Robots and Systems, 1992., Proceedings of the 1992 IEEE/RSJ International Conference on.
- [33] M. Grebenstein, M. Chalon, G. Hirzinger, and R. Siegwart, "Antagonistically driven finger design for the anthropomorphic dlr hand arm system," 2010, proc. IEEE-RAS International Conference on Humanoid Robots (HUMANOIDS).
- [34] H. Kobayashi, K. Hyodo, and D. Ogane, "On tendon-driven robotic mechanisms with redundant tendons," *The International Journal of Robotics Research*, vol. 17, no. 5, p. 561, 1998.
- [35] S. Huang and J. M. Schimmels, "The bounds and realization of spatial compliances achieved with simple serial elastic mechanisms," *Robotics and Automation, IEEE Transactions on*, vol. 16, no. 1, pp. 99–103, 2000.
- [36] J. J. Kutch and F. J. Valero-Cuevas, "Muscle redundancy does not imply robustness to muscle dysfunction," *Journal of Biomechanics*, vol. 44, no. 7, pp. 1264–1270, 2011.
- [37] L. W. Tsai and J. J. Lee, "Kinematic analysis of tendon-driven robotic mechanisms using graph theory," 1988.
- [38] A. Pashkevich, A. Klimchik, and D. Chablat, "Enhanced stiffness modeling of manipulators with passive joints," *Mechanism and machine theory*, 2011.
- [39] N. Hogan, "Mechanical impedance of single-and multi-articular systems," *Multiple muscle systems biomechanics and movement organization*, no. 9, pp. 1–23, 1990.
- [40] S. F. Chen and I. Kao, "Conservative congruence transformation for joint and cartesian stiffness matrices of robotic hands and fingers," *The International Journal of Robotics Research*, vol. 19, no. 9, pp. 835–847, 2000.
- [41] G. Alici and B. Shirinzadeh, "Enhanced stiffness modeling, identification and characterization for robot manipulators," *Robotics, IEEE Transactions on*, vol. 21, no. 4, pp. 554–564, 2005.
- [42] J. McIntyre, F. A. Mussa-Ivaldi, and E. Bizzi, "Modeling of multi-joint motor systems." IEEE, 1989, pp. 242–243 vol. 1, engineering in Medicine and Biology Society, 1989. Images of the Twenty-First Century., Proceedings of the Annual International Conference of the IEEE Engineering in.
- [43] —, "The control of stable postures in the multijoint arm," *Experimental brain research*, vol. 110, no. 2, pp. 248–264, 1996.
- [44] S. Stroeve, "Impedance characteristics of a neuromusculoskeletal model of the human arm i. posture control," *Biological cybernetics*, vol. 81, no. 5, pp. 475–494, 1999.
- [45] L. Elsner, C. He, and V. Mehrmann, "Minimization of the norm, the norm of the inverse and the condition number of a matrix by completion," *Numerical linear algebra with applications*, vol. 2, no. 2, pp. 155–171, 1995.
- [46] Z. Lu and T. K. Pong, "Minimizing condition number via convex programming," 2010.
- [47] X. Chen, R. S. Womersley, and J. Ye, "Minimizing the condition number of a gram matrix," *SIAM J. Optim*, vol. 21, p. 127148, 2011.
- [48] F. J. Valero-Cuevas, "A mathematical approach to the mechanical capabilities of limbs and fingers," *Progress in Motor Control*, pp. 619–633, 2005.
- [49] J. L. Fu and N. S. Pollard, "On the importance of asymmetries in grasp quality metrics for tendon driven hands," 2006, pp. 1068–1075, 2006 IEEE/RSJ International Conference on Intelligent Robots and Systems.
- [50] C. B. Barber, D. P. Dobkin, and H. Huhdanpaa, "The quickhull algorithm for convex hulls," *ACM Transactions on Mathematical Software (TOMS)*, vol. 22, no. 4, pp. 469–483, 1996.
- [51] F. J. Valero-Cuevas, V. V. Anand, A. Saxena, and H. Lipson, "Beyond parameter estimation: Extending biomechanical modeling by the explicit exploration of model topology," *Biomedical Engineering, IEEE Transactions on*, vol. 54, no. 11, pp. 1951–1964, 2007.